

Neutron scattering study on $\text{La}_{1.9}\text{Ca}_{1.1}\text{Cu}_2\text{O}_{6+\delta}$ and $\text{La}_{1.85}\text{Sr}_{0.15}\text{CaCu}_2\text{O}_{6+\delta}$

M. Hücker, Young-June Kim, G. D. Gu, and J. M. Tranquada
Physics Department, Brookhaven National Laboratory, Upton, New York 11973, USA

B. D. Gaulin
Department of Physics and Astronomy, McMaster University, Hamilton, Ontario, Canada L8S 4M1

J. W. Lynn
NIST Center for Neutron Research, National Institute of Standards and Technology, Gaithersburg, Maryland 20742, USA
 (Dated: February 2, 2008)

We present neutron scattering data on two single crystals of the high temperature superconductor $\text{La}_{2-x}(\text{Ca}, \text{Sr})_x\text{CaCu}_2\text{O}_{6+\delta}$. The $\text{Ca}_{0.1}$ -doped crystal exhibits a long-range antiferromagnetically ordered ground state. In contrast, the $\text{Sr}_{0.15}$ -doped crystal exhibits short-range antiferromagnetic order as well as weak superconductivity. In both crystals antiferromagnetic correlations are commensurate; however, some results on the $\text{Ca}_{0.1}$ -doped crystal resemble those on the spin-glass phase of $\text{La}_{2-x}\text{Sr}_x\text{CuO}_4$, where magnetic correlations became incommensurate. In addition, both crystals show a structural transition from tetragonal to orthorhombic symmetry. Quite remarkably, the temperature dependence and correlation length of the magnetic order is very similar to that of the orthorhombic distortion. We attribute this behavior to an orthorhombic strain-induced inter-bilayer magnetic coupling, which triggers the antiferromagnetic order. The large size of the crystals made it also possible to study the magnetic diffuse scattering along rods perpendicular to the CuO_2 planes in more detail. For comparison we show X-ray diffraction and magnetization data. In particular, for the $\text{Ca}_{0.1}$ -doped crystal these measurements reveal valuable information on the spin-glass transition as well as a second anomaly associated with the Néel transition.

PACS numbers: 74.72.Dn, 74.25.Ha, 61.12.-q

I. INTRODUCTION

The system $\text{La}_2\text{CaCu}_2\text{O}_{6+\delta}$ is a very interesting member of the family of high temperature superconductors. Similar to $\text{YBa}_2\text{Cu}_3\text{O}_{6+\delta}$ it has CuO_2 bilayers. However, it has no CuO chain-layers.¹ To introduce hole-like charge carriers into the CuO_2 planes it can be doped with Sr and Ca, although specimens generally have to be annealed under high oxygen pressure to become bulk superconductors.^{2,3,4} The maximum T_c of ~ 60 K is relatively low compared to other bilayer systems.⁵ High pressure oxygen annealing was shown to introduce interstitial oxygen, which leads to an increase of the hole concentration.^{3,6} Furthermore, it increases the miscibility range for Sr and Ca doping.³ The detailed role of the oxygen interstitials, in particular with respect to superconductivity, is still unclear.

So far, most studies were performed on polycrystalline specimens, which are much easier to homogeneously charge with oxygen than are the large single crystals needed for neutron scattering. However, the study of underdoped crystals grown at low oxygen pressure is as important as the study of bulk superconductors, since high temperature superconductivity at high hole doping seems to be intimately connected with the antiferromagnetic correlations at low hole doping.⁷ In particular, there is growing evidence that incommensurate antiferromagnetic correlations of the Cu spins are associated with the so-called charge and spin stripes, which may play a vital role for su-

perconductivity.^{8,9,10,11,12,13,14,15,16,17} In a recent neutron diffraction experiment on a non-superconducting $\text{La}_{1.80}\text{Sr}_{0.20}\text{CaCu}_2\text{O}_{6+\delta}$ single crystal grown at 1 atm oxygen pressure a commensurate short-range antiferromagnetic order was observed.¹⁸ This finding is in sharp contrast to the incommensurate spin stripes found in $\text{La}_{2-x}\text{Sr}_x\text{CuO}_4$ with comparable hole concentration.^{19,20} The present study is aimed at a better understanding of the different behavior in $\text{La}_{2-x}(\text{Sr}, \text{Ca})_x\text{CaCu}_2\text{O}_{6+\delta}$.

Structurally, $\text{La}_{2-x}(\text{Sr}, \text{Ca})_x\text{CaCu}_2\text{O}_{6+\delta}$ is known as the most simple bilayer system.^{1,2} Its unit cell, displayed in Fig. 1, can be derived from that of the single layer sister compound $\text{La}_{2-x}\text{Sr}_x\text{CuO}_4$ by replacing the CuO_6 octahedral network by two CuO_5 pyramidal planes, separated by a cation monolayer. In a stoichiometric compound ($\delta = 0$) the interstitial oxygen site O(3) is not occupied.²¹ The structure of the rocksalt layers separating adjacent bilayers is identical to those in $\text{La}_{2-x}\text{Sr}_x\text{CuO}_4$. In the undoped case ($x = 0$), one would ideally expect that the lattice site M(1) in the center of a bilayer is occupied by Ca, and the lattice site M(2) in the rock salt layers by La [Fig. 1]. However, it turns out that about 10% of the M(1) sites are occupied by La, while a corresponding number of alkaline earths go on the M(2) site.^{6,18,22,23} This ratio will of course change slightly upon doping Sr or Ca for La. Interstitial oxygen introduced by high pressure oxygen annealing goes on the O(3) site, and effectively bridges two CuO_5 pyramids in a bilayer to two CuO_6 octahedra, coupled via their apical oxygen.^{3,6,24,25,26}

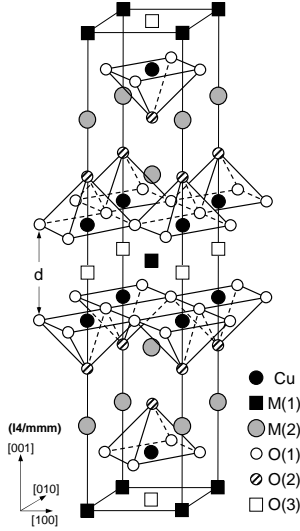


FIG. 1: Unit cell of $\text{La}_{2-x}(\text{Sr}, \text{Ca})_x\text{CaCu}_2\text{O}_{6+\delta}$ in the tetragonal high temperature phase.

In this work we present neutron scattering results on two large single crystals with the compositions $\text{La}_{1.9}\text{Ca}_{1.1}\text{Cu}_2\text{O}_{6+\delta}$ and $\text{La}_{1.85}\text{Sr}_{0.15}\text{CaCu}_2\text{O}_{6+\delta}$. Optical conductivity measurements by Wang et al.²⁷ have shown that both compounds contain a significant hole concentration p per CuO_2 plane, roughly consistent with the nominal values $p = x/2$. [Note that for $\text{La}_{2-x}\text{Sr}_x\text{CuO}_4$ $p = x$.] From neutron diffraction (ND) we find that the Ca-doped crystal exhibits a long-range antiferromagnetic order. In contrast, the Sr-doped crystal exhibits a short-range antiferromagnetic order as well as weak superconductivity, with $T_c^{\text{onset}} \sim 25$ K and a superconducting volume fraction of the order of one percent. In both crystals antiferromagnetism is commensurate, which is not surprising for the long-range order, but somewhat unexpected in the case of the Sr-doped crystal. In addition, both crystals show a structural transition from a high-temperature-tetragonal phase to a low-temperature-orthorhombic phase, first identified in Ref. 18. The temperature dependence of the magnetic order and the orthorhombic lattice distortion show a remarkable similarity, which we discuss in terms of a distortion induced magnetic inter-bilayer coupling. It is possible that this magneto-elastic coupling influences the electronic ground state and maybe even determines whether it is magnetic or superconducting. The large size of the crystals made it possible to study the elastic and inelastic response from two dimensional (2D) diffuse scattering, which shows up in rods along Q_z . Furthermore, we have performed a number of X-ray diffraction (XRD) measurements, which reveal additional information about the temperature dependence of the line width of the orthorhombic superlattice peak in both crystals (Sec. III B). Measurements of the static magnetic susceptibility reveal information about the spin-glass transition, and show a second anomaly associated with the antifer-

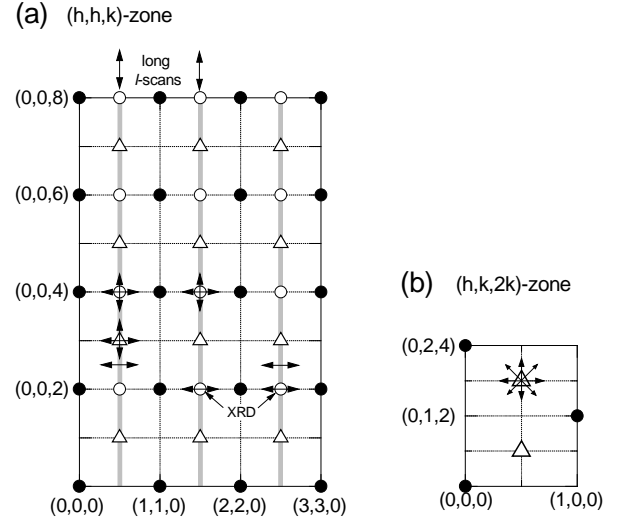


FIG. 2: Reciprocal space for the (h, h, l) and $(h, k, 2k)$ zones with typical scans indicated by arrows. X-ray diffraction experiments (XRD) where mainly performed at $(\frac{3}{2}, \frac{3}{2}, 2)$ and $(\frac{5}{2}, \frac{5}{2}, 2)$.

romagnetic order in the Ca-doped crystal (Sec. III C).

II. EXPERIMENTAL

The two centimeter-size single crystals with \varnothing 6-7 mm and length of ~ 10 cm were grown at Brookhaven and McMaster University by the travelling-solvent floating-zone method. The $\text{La}_{1.9}\text{Ca}_{1.1}\text{Cu}_2\text{O}_{6+\delta}$ crystal was grown in an atmosphere of flowing oxygen gas at a pressure of $p(\text{O}_2) = 1$ atm. The $\text{La}_{1.85}\text{Sr}_{0.15}\text{CaCu}_2\text{O}_{6+\delta}$ crystal was grown at $p(\text{O}_2) = 11$ atm, to increase the concentration of oxygen interstitials. At the given pressures, both compositions are within the range for single-phase solid solutions of this material.³ Our attempts to grow crystals with $x \geq 0.2$ and $p(\text{O}_2) = 11$ atm inevitably yielded samples containing a second phase.

In the case of $\text{La}_{1.9}\text{Ca}_{1.1}\text{Cu}_2\text{O}_{6+\delta}$, neutron scattering experiments were performed on two large pieces with weights of 3.9 g and 5.3 g. For $\text{La}_{1.85}\text{Sr}_{0.15}\text{CaCu}_2\text{O}_{6+\delta}$ the studied piece had a weight of 5.1 g. As mentioned earlier, this crystal shows weak superconductivity, although it has a lower Sr content than the crystal studied in Ref. 18, which was grown at $p(\text{O}_2) = 1$ atm and insulating at low temperatures. We associate this different behavior with the higher oxygen pressure used in our crystal growth procedure.

The neutron scattering experiments were carried out on the triple-axis spectrometer BT9 at the NIST Center for Neutron Research, at neutron energies of 14.7 meV and 30.5 meV. Pyrolytic graphite (PG) (002) reflections were used for both the monochromator and the analyzer. To eliminate higher-order contamination, an additional PG filter was put into the beam after the analyzer. The

crystals were mounted in a He filled Al can. X-ray diffraction experiments were performed in reflection at beam-line X22C of the National Synchrotron Light Source at Brookhaven at a photon energy of 8.9 keV. The magnetization of small pieces of the crystals was measured with a SQUID (superconducting quantum interference device) magnetometer.

III. RESULTS AND DISCUSSION

Figure 2(a) shows the reciprocal space for the (h, h, l) zone of $\text{La}_2\text{CaCu}_2\text{O}_{6+\delta}$ in the notation of the tetragonal unit cell of Fig. 1 with space group $I4/mmm$. At room temperature both crystals are tetragonal and only fundamental Bragg peaks (\bullet) are observed. At low temperatures additional peaks appear, indicating the transition into the orthorhombic phase¹⁸ (\circ) as well as static antiferromagnetic order (Δ). Note that magnetic Bragg peaks are allowed for $l = n$ ($n \neq 0$) but for l even they are dominated by the nuclear superlattice peaks.^{28,29} In the orthorhombic phase, with space group $Bmab$, no splitting of the in-plane lattice constants was observed within the resolution of the neutron and X-ray experiments, although X-ray data show a clear broadening of corresponding fundamental Bragg peaks for in-plane momentum transfers. This suggests that the orthorhombic strain is weak, i.e., much weaker than in $\text{La}_{2-x}\text{Sr}_x\text{CuO}_4$.^{30,31} Therefore, throughout this paper reflections will be indexed using the notation for the tetragonal unit cell and scattering vectors $\mathbf{Q} = (h, k, l)$ will be specified in units of $(2\pi/a, 2\pi/a, 2\pi/c)$. The thick grey lines in Fig. 2(a) symbolize scattering rods along the c -axis from 2D scattering. The arrows mark the positions where most of the scans were performed. To test whether the magnetic Bragg peaks are incommensurate, the crystal was mounted in the $(h, k, 2k)$ zone where all scans were performed on the $(\frac{1}{2}, \frac{3}{2}, 3)$ peak [see Fig. 2(b)]. For the lattice parameters at ~ 10 K, as determined by neutron diffraction, we find $a = 3.82(1)$ Å and $c = 19.41(5)$ Å for $\text{La}_{1.85}\text{Sr}_{0.15}\text{CaCu}_2\text{O}_{6+\delta}$, as well as $a = 3.83(1)$ Å and $c = 19.36(5)$ Å for $\text{La}_{1.9}\text{Ca}_{1.1}\text{Cu}_2\text{O}_{6+\delta}$.

A. Neutron Scattering

1. Magnetic Bragg and orthorhombic superlattice peaks

In Fig. 3(a) we show long l -scans along $\mathbf{Q} = (\frac{1}{2}, \frac{1}{2}, l)$ and $(\frac{3}{2}, \frac{3}{2}, l)$ for $\text{La}_{1.9}\text{Ca}_{1.1}\text{Cu}_2\text{O}_{6+\delta}$ at low temperatures [cf. Fig. 2(a)]. One can clearly see the increase of the predominantly nuclear superlattice peaks for $l = 2n$ ($n \neq 0$) as well as the decrease of the purely magnetic Bragg peaks for l odd with increasing $|\mathbf{Q}|$. As mentioned earlier there is also a small magnetic contribution for l even. Weak intensity observed at $l = 0$ is believed to arise from higher harmonics or multiple scattering. Note that in contrast to La_2CuO_4 no magnetic peak is expected at

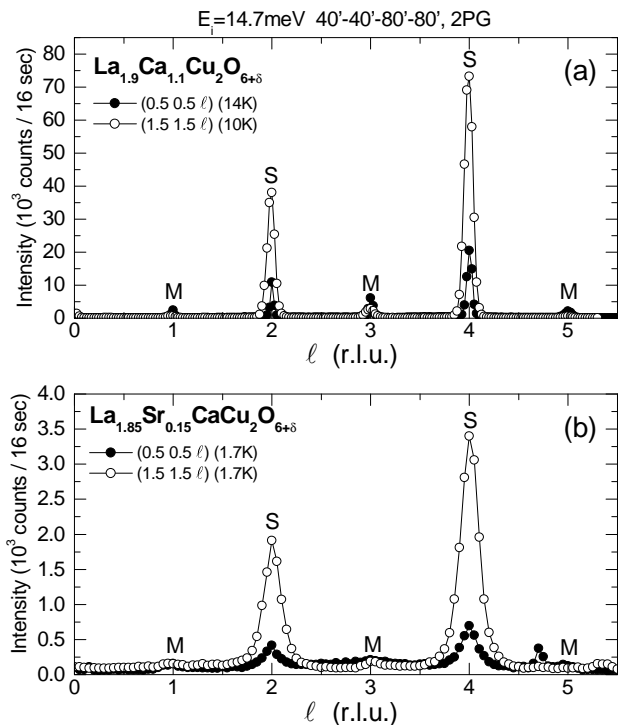


FIG. 3: Elastic scans along $\mathbf{Q} = (\frac{1}{2}, \frac{1}{2}, l)$ and $(\frac{3}{2}, \frac{3}{2}, l)$ for $\text{La}_{1.9}\text{Ca}_{1.1}\text{Cu}_2\text{O}_{6+\delta}$ (top) and $\text{La}_{1.85}\text{Sr}_{0.15}\text{CaCu}_2\text{O}_{6+\delta}$ (bottom). M indicates magnetic Bragg reflections and S predominantly nuclear superlattice reflections.

$l = 0$, since the magnetic structure factor is zero (see Sec. III A 2).^{28,29} The peak width in Fig. 3(a) is resolution limited. From h -scans through the magnetic $(\frac{1}{2}, \frac{1}{2}, 1)$ peak with a collimation of $10'-10'-10'-10'$ (not shown) we have extracted a minimum in-plane correlation length of $\xi \simeq 270$ Å, suggesting that $\text{La}_{1.9}\text{Ca}_{1.1}\text{Cu}_2\text{O}_{6+\delta}$ exhibits a long-range antiferromagnetic order.³² In the case of $\text{La}_{1.85}\text{Sr}_{0.15}\text{CaCu}_2\text{O}_{6+\delta}$ in Fig. 3(b) the peak intensities are about one order of magnitude smaller and the peak widths much larger, indicating a short-range order. For the structural distortion we find that in-plane and out-of-plane correlation lengths are about the same and of the order of $\xi \simeq 27$ Å. Interestingly, the in-plane correlation length of the magnetic order is nearly identical with this, as will be shown below in more detail. However, the magnetic peaks are too weak to extract a reliable value for the correlation length along c .

Fig. 4 shows the intensity of representative magnetic and structural superlattice peaks, after subtraction of the background, as a function of temperature. First we will focus on $\text{La}_{1.9}\text{Ca}_{1.1}\text{Cu}_2\text{O}_{6+\delta}$, which we have studied twice. In the first experiment (#1), the intensity of the magnetic $(\frac{1}{2}, \frac{1}{2}, 3)$ peak in Fig. 4(a) indicates Néel ordering above room temperature. However, the relatively slow increase of the intensity below T_N suggests that the phase transition is quite inhomogeneous. In addition, two further transitions are observed: one at ~ 175 K, where the intensity starts to increase faster, and a second at

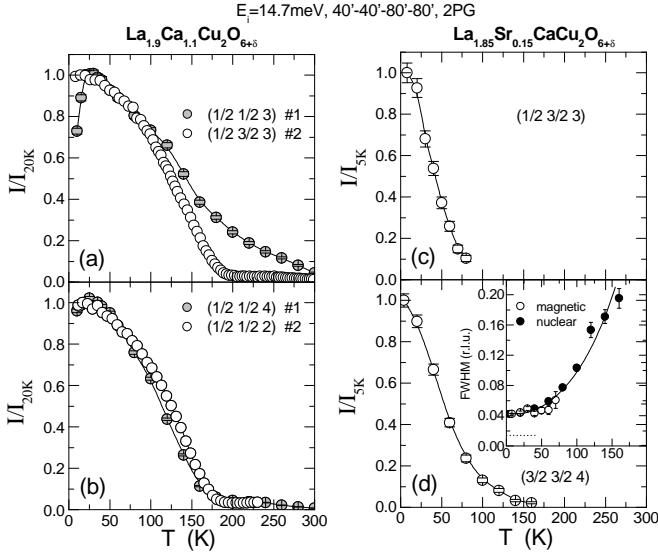


FIG. 4: Intensity of the magnetic Bragg peaks $(\frac{1}{2}, \frac{1}{2}, 3)$ and $(\frac{1}{2}, \frac{3}{2}, 3)$, and the orthorhombic superlattice peaks $(\frac{1}{2}, \frac{1}{2}, 4)$, $(\frac{1}{2}, \frac{1}{2}, 2)$, and $(\frac{3}{2}, \frac{3}{2}, 4)$, of $\text{La}_{1.9}\text{Ca}_{1.1}\text{Cu}_2\text{O}_{6+\delta}$ (a, b) and $\text{La}_{1.85}\text{Sr}_{0.15}\text{CaCu}_2\text{O}_{6+\delta}$ (c, d) as a function of temperature. #1 and #2 denote data from different experiments (see text). In (a) and (b) errors are within point size. Inset: Full width at half maximum of magnetic Bragg and orthorhombic superlattice peaks in $\text{La}_{1.85}\text{Sr}_{0.15}\text{CaCu}_2\text{O}_{6+\delta}$ as a function of temperature. Spectrometer resolution indicated by dotted line.

20 K, where the intensity decreases. In a second experiment (#2) performed three months later on the same crystal as well as on a second crystal, T_N had decreased to ~ 175 K, though also in this case a very weak peak could be traced up to 300 K. Moreover, the drop in intensity below 20 K appeared to be weaker by a factor of 2-3. We note that we have checked this for the same crystal, peak and spectrometer configuration as in experiment #1. However, a full temperature scan was performed only on the $(\frac{1}{2}, \frac{3}{2}, 3)$ peak after mounting this crystal in the $(h, k, 2k)$ zone [Fig. 4(a)]. Surprisingly, in this case the drop below 20 K is not observed at all. We explain this as follows: with the crystal mounted in the $(h, k, 2k)$ zone the 2D scattering rods are almost perpendicular to the horizontal scattering plane. Because of the relaxed collimation in the vertical direction, scans through the magnetic Bragg peak will also integrate some intensity from 2D scattering. As the diffuse intensity increases at low temperature (Sec. III A 2) it possibly compensates the decrease of the magnetic Bragg peak below 20 K.

The clear decrease of the magnetic peak intensity below 20 K in experiment #1 strongly resembles findings for the spin-glass phase in lightly Sr-doped $\text{La}_{2-x}\text{Sr}_x\text{CuO}_4$ with $x < 0.02$.³³ There, the decrease of the commensurate magnetic Bragg peak is accompanied by the appearance of intensity at peak positions consistent with incommensurate stripe antiferromagnetism.³³ Unfortunately, the apparent change of our sample prevented us from taking similar measurements on $\text{La}_{1.9}\text{Ca}_{1.1}\text{Cu}_2\text{O}_{6+\delta}$

in the same state as that found in experiment #1. In the second experiment no intensity at incommensurate peak positions was observed (see Sec. III A 3). Although further experiments are needed to sort out why the sample has changed, a very likely scenario is a redistribution of the oxygen over time.

In contrast to the magnetic peaks, the temperature dependence of the orthorhombic superlattice peaks of $\text{La}_{1.9}\text{Ca}_{1.1}\text{Cu}_2\text{O}_{6+\delta}$ are nearly identical in both experiments [Fig. 4(b)]. Below the structural transition at 175 K intensity increases and saturates at low temperatures. It may, however, be important to notice that in experiment #1 the intensity slightly decreases below 20 K. We assume that this decrease is caused by the magnetic contribution to the $(\frac{1}{2}, \frac{1}{2}, 4)$ peak, which is about 15-20%.

Quite remarkably, the temperature profiles of magnetic and superstructure peaks in experiment #2 are almost identical [cf. Fig. 4(a) and (b)], indicating a magneto-elastic coupling. The same similarity is observed for the $\text{La}_{1.85}\text{Sr}_{0.15}\text{CaCu}_2\text{O}_{6+\delta}$ crystal in Fig. 4(c) and (d), with the major differences being that the transition occurs at around 125 K and the order is short-range. The lower transition temperature and much weaker peak intensity most likely follows from the higher hole and oxygen content than in $\text{La}_{1.9}\text{Ca}_{1.1}\text{Cu}_2\text{O}_{6+\delta}$. We mention that similar data as for our $\text{La}_{1.85}\text{Sr}_{0.15}\text{CaCu}_2\text{O}_{6+\delta}$ crystal were obtained by Ulrich et al. on a $\text{La}_{1.80}\text{Sr}_{0.20}\text{CaCu}_2\text{O}_{6+\delta}$ crystal with short-range order.¹⁸ However, our results on $\text{La}_{1.9}\text{Ca}_{1.1}\text{Cu}_2\text{O}_{6+\delta}$ show that the coupling of orthorhombic strain and antiferromagnetic order also exists in samples with low charge carrier concentration and long-range order (see discussion).

The inset in Fig. 4(d) shows the full width at half maximum of the magnetic and the orthorhombic in-plane peak width in reciprocal lattice units of $a^* = 2\pi/a$. The contribution of the spectrometer resolution to the line width at the lowest temperature amounts to 5%. While the orthorhombic superlattice peak could be analyzed up to 160 K, the magnetic peak became too weak for $T > 70$ K. Nevertheless, it is obvious that up to 70 K the magnetic peak width is nearly the same as for the structural peak, and shows a similar temperature dependence. For a comparison of the width of the orthorhombic superlattice peaks in both of the crystals, we refer to Sec. III B, where we show high-resolution X-ray diffraction results.

2. Diffuse scattering

A closer look at the data of $\text{La}_{1.9}\text{Ca}_{1.1}\text{Cu}_2\text{O}_{6+\delta}$ reveals significant intensity from elastic 2D scattering between the Bragg peaks (Fig. 5). At low $|\mathbf{Q}|$ it originates largely from magnetic scattering, as will be discussed in the next paragraph. The long l -scan in Fig. 5(a), which is the same as in Fig. 3(a), shows that the 2D magnetic scattering intensity is modulated sinusoidally. [Note that the

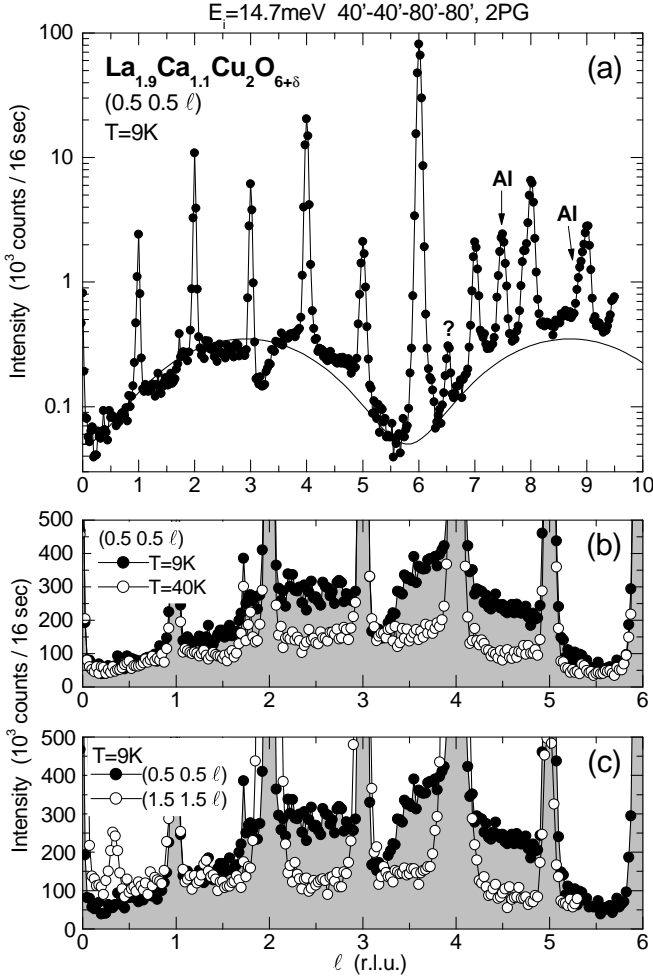


FIG. 5: Elastic l -scans for $\text{La}_{1.9}\text{Ca}_{1.1}\text{Cu}_2\text{O}_{6+\delta}$. (a) along $\mathbf{Q} = (\frac{1}{2}, \frac{1}{2}, l)$ at 9 K (logarithmic intensity scale). The peak at $l = 7.46$ as well as the left shoulder of the peak at $l = 9$ originate from Al powder ring reflections. (b) along $\mathbf{Q} = (\frac{1}{2}, \frac{1}{2}, l)$ at 9 K and 40 K. (c) along $\mathbf{Q} = (\frac{1}{2}, \frac{1}{2}, l)$ and $(\frac{3}{2}, \frac{3}{2}, l)$ at 9 K. The origin of the peaks at $l = 6.5$ in (a) and at $l = 0.35$ in (c) is not clear, but there seems to be no systematic appearance of further unidentified peaks.

dip in the data at $l = 3.2$ was not reproducible, e.g., in an identical scan in Fig. 6(b) it is absent.] The modulation results from the antiferromagnetic coupling between the CuO_2 planes within a bilayer and is proportional to the square of the magnetic structure factor $g(\mathbf{q})$ for the acoustic spin wave mode:^{13,34,35}

$$g = \sin(\pi z l) \quad (1)$$

where z is the ratio between the intra-bilayer distance d of the CuO_2 planes and the lattice parameter c (see Fig. 1). For lightly Ca- or Sr-doped $\text{La}_2\text{CaCu}_2\text{O}_{6+\delta}$ the literature^{6,18} gives a value of $z \simeq 0.17$, resulting in the solid line in Fig. 5, which is in good agreement with the modulation of the data. The first maximum of the magnetic structure factor is reached for $l = 2.9$, which is why magnetic Bragg peaks are studied best at $l = 3$.

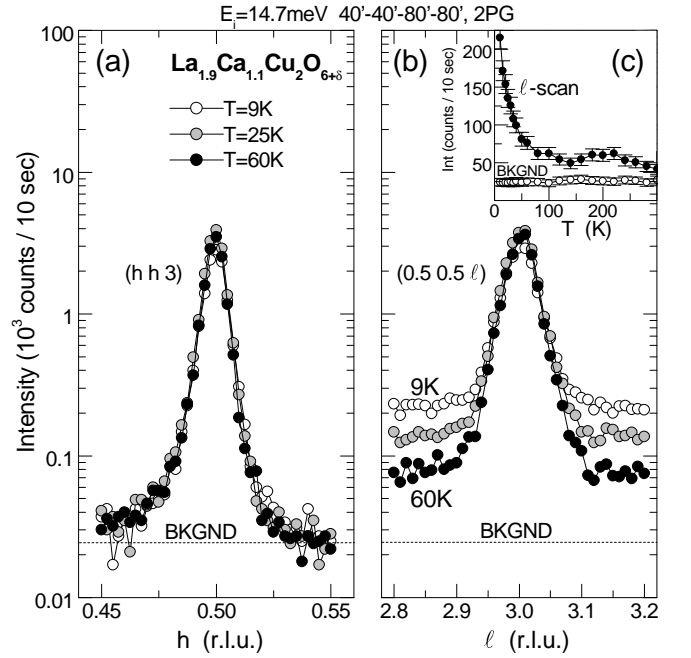


FIG. 6: Elastic scans through the magnetic Bragg peak $(\frac{1}{2}, \frac{1}{2}, 3)$ of $\text{La}_{1.9}\text{Ca}_{1.1}\text{Cu}_2\text{O}_{6+\delta}$ at different temperatures. (a) h -scans. (b) l -scans. (c) background signal as well as diffuse scattering intensity extracted from h - and l -scans.

Note that for a detailed description of the scattering intensity one has to include the magnetic form factor and the spin structure, as well as the spectrometer resolution, which we have neglected in this qualitative discussion.³⁴ The magnetic form factor is a slowly varying function and causes a decrease of intensity with increasing $|\mathbf{Q}|$.³⁵ On the other hand, assuming a collinear spin structure with the spins lying within the CuO_2 planes (as in other cuprates), we expect an increase of intensity with increasing l associated with an increase of the magnetic interaction vector $\mathbf{S}_\perp = \hat{\mathbf{Q}} \times (\mathbf{S} \times \hat{\mathbf{Q}})$, where \mathbf{S} is the Cu spin and $\hat{\mathbf{Q}} = \mathbf{Q}/|\mathbf{Q}|$.³⁶ The l dependence of \mathbf{S}_\perp most likely explains why in Fig. 5(a) the 2D scattering intensity around the second maximum at $l = 8.7$ is higher than around the first maximum at $l = 2.9$.³⁷

The elastic 2D magnetic scattering intensity strongly decreases with increasing temperature as can be seen from Fig. 5(b) where we show a comparison of l -scans at 9 K and 40 K. A more detailed temperature dependence was extracted from scans through the magnetic $(\frac{1}{2}, \frac{1}{2}, 3)$ peak in Fig. 6(a) and (b). In h -scans, the intensity in the tails at any temperature quickly approaches the background, while in l -scans it stays above the background due to 2D scattering. When increasing the temperature up to ~ 100 K, the 2D scattering intensity drastically decreases, but stays above background up to room temperature [Fig. 6(c)].

It is important to notice that the temperature dependence of the diffuse scattering intensity in Fig. 6(c) is different from that of the magnetic Bragg peaks in

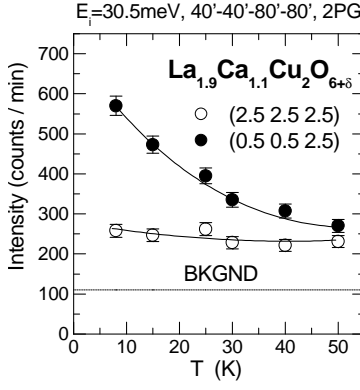


FIG. 7: Elastic diffuse scattering intensity at $(\frac{1}{2}, \frac{1}{2}, \frac{5}{2})$ and $(\frac{5}{2}, \frac{5}{2}, \frac{5}{2})$ in $\text{La}_{1.9}\text{Ca}_{1.1}\text{Cu}_2\text{O}_{6+\delta}$ as a function of temperature.

Fig. 4(a). Instead it is more similar to the temperature dependence of the short-range magnetic order in $\text{La}_{1.85}\text{Sr}_{0.15}\text{CaCu}_2\text{O}_{6+\delta}$ in Fig. 4(c). The increase of the diffuse intensity is particularly steep at temperatures where the decrease of the magnetic Bragg peak was observed, indicating that intensity is transferred from the Bragg peaks to the 2D scattering rods [cf. Fig. 6(c) and 4(a)]. A similar transfer of intensity at low temperatures was observed in $\text{La}_{2-x}\text{Sr}_x\text{CuO}_4$ with $x < 0.02$ (Ref. 33) and in $\text{YBa}_2\text{Cu}_3\text{O}_{6.3}$ (see Fig. 13 and 14 in Ref. 34). Therefore, we assume that it is associated with the freezing of spin fluctuations, which leads to the formation of the spin glass phase at low temperatures.

To examine the origin of the elastic 2D scattering, we have studied its $|\mathbf{Q}|$ dependence in $\text{La}_{1.9}\text{Ca}_{1.1}\text{Cu}_2\text{O}_{6+\delta}$. As is shown in Fig. 5(c), the diffuse scattering intensity in a scan along $\mathbf{Q} = (\frac{3}{2}, \frac{3}{2}, l)$ is significantly lower than in a scan along $\mathbf{Q} = (\frac{1}{2}, \frac{1}{2}, l)$, indicating that at low $|\mathbf{Q}|$ it results largely from 2D magnetic scattering. On the other hand, h -scans along $\mathbf{Q} = (h, h, \frac{5}{2})$ through the 2D scattering rods at $h = \frac{1}{2}$ and $h = \frac{5}{2}$ reveal that some of the intensity results from 2D nuclear scattering. In Fig. 7, where we show intensities, one can see that the intensity at $\mathbf{Q} = (\frac{1}{2}, \frac{1}{2}, \frac{5}{2})$ decreases with increasing temperature, while at $\mathbf{Q} = (\frac{5}{2}, \frac{5}{2}, \frac{5}{2})$ it is temperature independent, indicating the dominance of 2D nuclear scattering for higher $|\mathbf{Q}|$.

In $\text{La}_{1.85}\text{Sr}_{0.15}\text{CaCu}_2\text{O}_{6+\delta}$ the elastic 2D scattering intensity at 1.7 K is significantly weaker than in $\text{La}_{1.9}\text{Ca}_{1.1}\text{Cu}_2\text{O}_{6+\delta}$ at 9 K. It is modulated sinusoidally along l and decreases rapidly with increasing temperature. The period is the same as for the Ca-doped crystal in Fig. 5. In $\text{La}_{1.85}\text{Sr}_{0.15}\text{CaCu}_2\text{O}_{6+\delta}$ the modulation is particularly pronounced in inelastic scans, as is shown in Fig. 8 for scans along $\mathbf{Q} = (\frac{1}{2}, \frac{1}{2}, l)$ at 30 K and 200 K and an energy transfer of $\hbar\omega = 6$ meV. Note that this underlines the magnetic nature of the diffuse scattering, as at finite energies no significant contribution from diffuse nuclear scattering is expected. From Fig. 8 it is obvious that the modulation of the inelastic scattering intensity

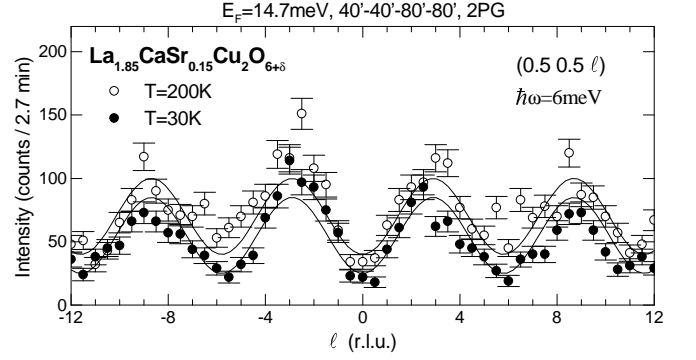


FIG. 8: Inelastic scans with $\hbar\omega = 6$ meV along $\mathbf{Q} = (\frac{1}{2}, \frac{1}{2}, l)$ for $\text{La}_{1.85}\text{Sr}_{0.15}\text{CaCu}_2\text{O}_{6+\delta}$.

far above and below the magnetic and structural transition at ~ 125 K does not differ significantly, indicating that in the paramagnetic phase the intra-bilayer antiferromagnetic correlations are still strong. We mention, that a similar structure factor modulation was observed in $\text{YBa}_2\text{Cu}_3\text{O}_{6+\delta}$.^{34,35} However, there the relative bilayer spacing amounts to $z = 0.28$, so that the first maximum is reached at $l = 1.8$, in comparison to $l = 2.9$ in $\text{La}_2\text{CaCu}_2\text{O}_{6+\delta}$. Furthermore, in $\text{YBa}_2\text{Cu}_3\text{O}_{6+\delta}$ it was observed that at $l = -1.8$ the intensity is larger than at $l = +1.8$, which is due to the so called focusing effect of the spectrometer resolution.³⁴ At $l = +1.8$ the long axis of the resolution ellipsoid has a significant angle with the 2D scattering rod, therefore integrating less intensity than at $l = -1.8$, where the long axis and the rod are approximately parallel. For $\text{La}_{1.85}\text{Sr}_{0.15}\text{CaCu}_2\text{O}_{6+\delta}$ in Fig. 8 the intensity at $l = -2.9$ is only slightly larger than at $l = +2.9$, which is due to the fact that the 2D scattering rod is relatively broad in h and k , which diminishes the focussing effect. Intensity clearly decreases with increasing l due to the magnetic form factor.

3. Search for spin stripes

In the presence of antiferromagnetic stripe correlations similar to those in $\text{La}_{2-x}\text{Sr}_x\text{CuO}_4$ we would expect intensity at incommensurate peak positions displaced by \mathbf{q}_s from the magnetic Bragg peaks at \mathbf{Q}_{AF} . Different sets of incommensurate peaks are possible, depending on whether the direction of stripes is parallel to the in-plane Cu-O bonds [$\mathbf{q}_s = (\pm\epsilon, 0, 0)$ or $(0, \pm\epsilon, 0)$] or diagonal [$\mathbf{q}_s = (\pm\sqrt{2}\epsilon, \pm\sqrt{2}\epsilon, 0)$ or $(\pm\sqrt{2}\epsilon, \mp\sqrt{2}\epsilon, 0)$].^{11,20,38} Since due to the magnetic structure factor the magnetic intensity is maximum near $l = 3$, the crystals were mounted in the $(h, k, 2k)$ zone, to scan these incommensurate positions around $\mathbf{Q}_{AF} = (\frac{1}{2}, \frac{3}{2}, 3)$ [see Fig. 2(b)]. For both stoichiometries, elastic scans at $T = 8$ K indicate commensurate antiferromagnetism. For the Sr-doped crystal the collimation was set to $40'-40'-80'-80'$, and for the Ca-doped crystal to $10'-20'-20'-20'$. Inelastic scans, performed on $\text{La}_{1.85}\text{Sr}_{0.15}\text{CaCu}_2\text{O}_{6+\delta}$ at $T = 8$ K, show

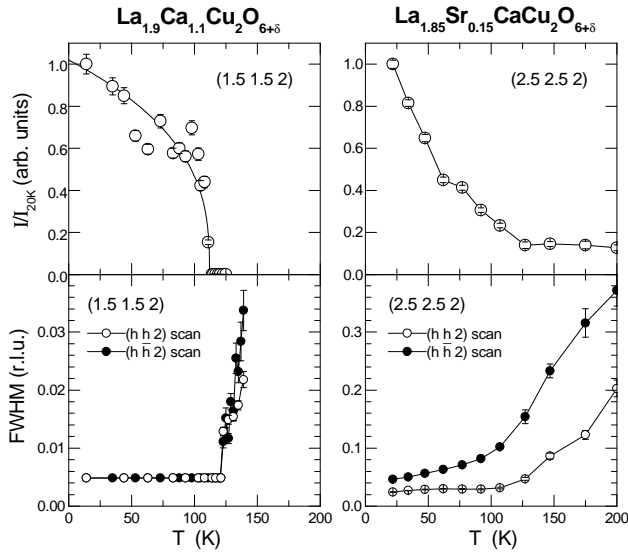


FIG. 9: Results from X-ray diffraction: Normalized integrated intensity and full width at half maximum of the orthorhombic superlattice peak $(\frac{5}{2}, \frac{5}{2}, 2)$ in $\text{La}_{1.9}\text{Ca}_{1.1}\text{Cu}_2\text{O}_{6+\delta}$ (left) and $\text{La}_{1.85}\text{Sr}_{0.15}\text{CaCu}_2\text{O}_{6+\delta}$ (right) as a function of temperature. Solid line in top left graph is a guide to the eye.

commensurate antiferromagnetism, also. These scans were performed at an energy transfer of $\hbar\omega = 3$ meV and a final energy of 14.7 meV. The $\text{La}_{1.9}\text{Ca}_{1.1}\text{Cu}_2\text{O}_{6+\delta}$ crystal was then mounted in the $(h, 3k, 7k)$ zone to perform elastic scans at $T = 8$ K through the 2D scattering rod at $\mathbf{Q} = (\frac{1}{2}, \frac{3}{2}, \frac{7}{2})$, with the collimation set to $40'-40'-80'-80'$ (this type of scans is not indicated in Fig. 2).³⁹ The scans show that the 2D magnetic scattering is commensurate, as well.

B. X-ray Diffraction

In Fig. 9 we show single crystal X-ray diffraction data on the orthorhombic superlattice peak. The polished surface of each crystal was mounted so that h -scans along $\mathbf{Q} = (h, h, l)$ as well as (h, \bar{h}, l) could be performed with high resolution. Interestingly, in $\text{La}_{1.9}\text{Ca}_{1.1}\text{Cu}_2\text{O}_{6+\delta}$ the structural phase transition is much sharper and takes place at a lower temperature (~ 115 K) than in the neutron scattering experiment (~ 170 K) [Fig. 4(a)]. Below the transition the line width is limited by the spectrometer resolution but significantly increases above the transition. For $\text{La}_{1.85}\text{Sr}_{0.15}\text{CaCu}_2\text{O}_{6+\delta}$ we observe a broad continuous transition with a critical temperature around 125 K, very similar to the neutron diffraction data in Fig. 4. The peak width is about one order of magnitude larger than that in $\text{La}_{1.9}\text{Ca}_{1.1}\text{Cu}_2\text{O}_{6+\delta}$, and its temperature dependence is in good agreement with our results from neutron diffraction. Although above the transition temperature intensity is very small, with X-rays the superlattice peak could be followed up to 200 K revealing a strong increase of the peak width. In both

crystals the superlattice peaks are sharper for h -scans along $\mathbf{Q} = (h, h, l)$ than in the perpendicular direction $\mathbf{Q} = (h, \bar{h}, l)$. According to Ulrich et al. the structural distortion in the orthorhombic phase consists of a displacement of the apical oxygen O(2) along $[110]$ (cf. Fig. 1). Hence, our data seem to indicate a larger domain size along the displacement direction than in the perpendicular in-plane direction.

C. Static Susceptibility

To compare our results from diffraction with macroscopic magnetic properties we have measured the static susceptibility χ of small pieces of the crystals. First we will focus on the susceptibility of $\text{La}_{1.9}\text{Ca}_{1.1}\text{Cu}_2\text{O}_{6+\delta}$. Figure 10(a) shows its χ in $H = 1$ T and 7 T for H parallel to the c -axis as well as parallel to the two in-plane directions $[110]$ and $[1\bar{1}0]$, which are parallel to the orthorhombic a and b axis. Because of twinning these two in-plane directions are mixed, which is why we call them $ab1$ and $ab2$. From room temperature the susceptibility slightly decreases with decreasing T for all three directions, which is typical for a cuprate S=1/2, 2D-Heisenberg antiferromagnet with a superexchange coupling constant J of the order of 0.1 eV.^{40,41} The Curie-type increase at low temperatures usually follows from magnetic impurities such as defect Cu spins. The difference between $H \parallel c$ and $H \parallel ab$ of $\sim 1.4 \times 10^{-4}$ emu/mol is largely due to the Cu Van Vleck magnetism, i.e., $\sim 0.7 \times 10^{-4}$ emu/mol per CuO_2 plane, which is in good agreement with literature.^{42,43,44} For $H \parallel c$, no anomaly is observed at the antiferromagnetic ordering temperature, and data for 1 T and 7 T are nearly identical. However, for magnetic field parallel to the CuO_2 planes we find a weak field dependence as well as a small anisotropy between $H \parallel ab1$ and $ab2$. The anisotropy indicates that the crystal is partially detwinned. At a field of 7 T, however, the anisotropy has vanished.

Figures 10(b) and (c) show zero-field-cooled and field-cooled data for different H at low temperatures. While for $H \parallel c$ data are nearly reversible, clear differences, as well as a hump, are observed for $H \parallel ab1$ and $H \parallel ab2$ (not shown) indicating the occurrence of a spin-glass transition at ~ 13 K. This is in contrast to $\text{La}_{2-x}\text{Sr}_x\text{CuO}_4$ where the spin-glass transition is visible for $H \parallel c$, also.^{45,46}

The fact that in $\text{La}_{2-x}\text{Sr}_x\text{CuO}_4$ both the Néel and the spin-glass transition are clearly visible for $H \parallel c$ is connected to a weak out-of-plane Dzyaloshinsky-Moriya spin canting, which follows from the rotation of the CuO_6 octahedra in the orthorhombic phase.^{47,48} As mentioned earlier, in $\text{La}_{1.9}\text{Ca}_{1.1}\text{Cu}_2\text{O}_{6+\delta}$ the orthorhombic distortion consists primarily of a displacement of the apical oxygen O(2) along $[110]$, while the basal oxygens O(1) seem to stay in the CuO_2 plane.¹⁸ Hence, the absence of a signature at the Néel and the spin-glass transition for $H \parallel c$ in $\text{La}_{1.9}\text{Ca}_{1.1}\text{Cu}_2\text{O}_{6+\delta}$ might be interpreted as ev-

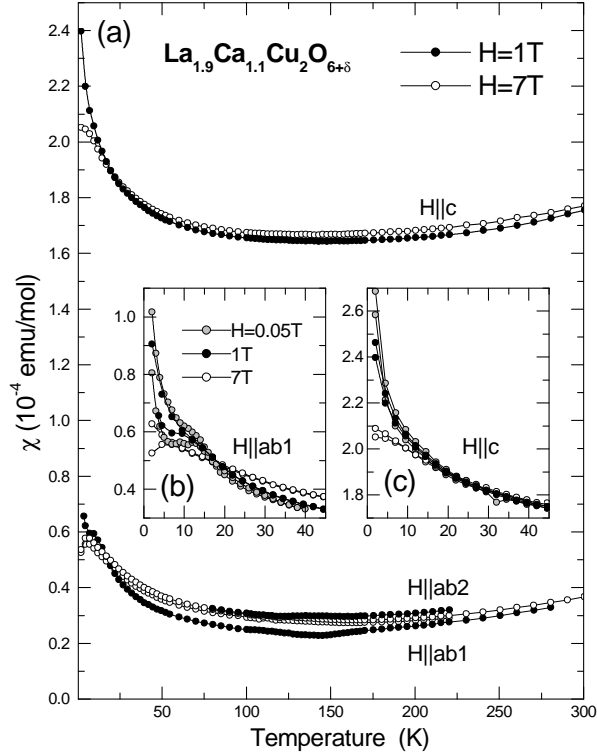


FIG. 10: Static magnetic susceptibility of $\text{La}_{1.9}\text{Ca}_{1.1}\text{Cu}_2\text{O}_{6+\delta}$ as a function of temperature and different directions of the applied field. (a) Zero field cooled data. (b), (c) Zero field cooled and field cooled data at low temperatures.

idence for the absence of an out-of-plane Dzyaloshinsky–Moriya spin canting. However, it can also mean that the Dzyaloshinsky–Moriya spin canting cancels due to a strong antiferromagnetic coupling between the CuO_2 planes of a bilayer. Since it is reasonable to assume that, similar to $\text{YBa}_2\text{Cu}_3\text{O}_{6+\delta}$, this interlayer coupling within a bilayer is orders of magnitude stronger than the inter-bilayer coupling, it will most likely be very difficult to test for the presence of a Dzyaloshinsky–Moriya spin canting by means of static magnetization measurements.^{47,48}

As is shown in Fig. 11 for magnetic field $H = 1$ T parallel to the CuO_2 planes, further anomalies are observed at ~ 115 K and ~ 160 K. In particular, for $H \parallel ab1$ these two temperatures border a dip-like anomaly, and for the perpendicular direction $H \parallel ab2$ a hump. In both cases the anomalies are suppressed by a magnetic field of the order of 4 – 5 T and at 7 T the susceptibility is isotropic (cf. Fig. 10). We mention that for $H = 1$ T applied parallel to $[100]$ no anomalies are observed; however, they can be induced at fields of 3 – 5 T and then disappear again at 7 T. Therefore, we assume that below T_N spins are either parallel to $[110]$ or $[1\bar{1}0]$ and the observed transitions as a function of field are due to a spin flop. The relatively low field scale indicates an in-plane spin wave gap of the order of 0.5 meV. This gap energy is much smaller than in La_2CuO_4 where the in-plane gap was associated with the Dzyaloshinsky–Moriya

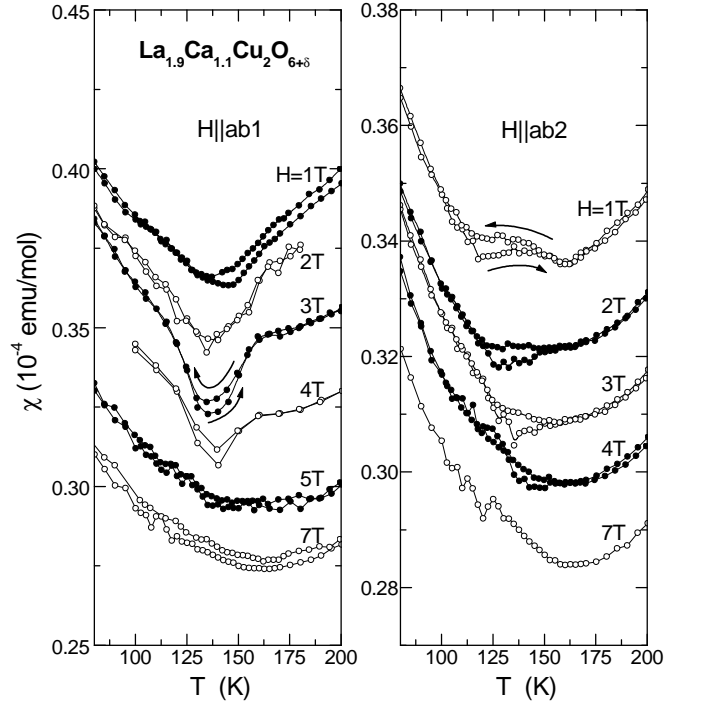


FIG. 11: Static magnetic susceptibility of $\text{La}_{1.9}\text{Ca}_{1.1}\text{Cu}_2\text{O}_{6+\delta}$ for different magnetic fields as a function of increasing and decreasing temperature. (a) for $H \parallel ab1$ and (b) for $H \parallel ab2$. Curves shifted for clarity.

spin canting, which might confirm that the spin canting in $\text{La}_2\text{CaCu}_2\text{O}_{6+\delta}$ is indeed small.^{49,50} For comparison, in La_2CuO_4 the spin flop field amounts to 10–15 T, and in tetragonal $\text{Sr}_2\text{CuO}_2\text{Cl}_2$ with perfectly coplanar spin structure it is only 0.7 T.^{51,52}

Interestingly, the two critical temperatures of 115 K and 160 K are nearly identical with the structural transition temperatures, as observed by XRD and ND, respectively (cf. Fig. 4 and 9). Considering our diffraction data alone, possible interpretations are (i) that we have indeed observed two distinct transitions, (ii) that surface effects are important (XRD), (iii) that an inhomogeneous distribution of the oxygen content exists. The fact that both anomalies show up in the macroscopic susceptibility indicates that they involve large volume fractions, making surface effects less likely. In the case of an inhomogeneous oxygen distribution we would expect one broad transition rather than two relatively sharp ones. On the other hand, for ND, probing the entire crystal, the transition is in fact relatively broad, while for XRD, probing a relatively small area of the sample, the transition is sharp. Hence, diffraction data are not inconsistent with an inhomogeneous oxygen distribution. In this case the anomaly at 115 K might correspond to the T_N of the hole rich surface region and the anomaly at 160 K the T_N of the bulk, which has a slightly lower average hole concentration. On the other hand, the susceptibility data in Fig. 11(a) are difficult to understand in terms of a sequence of two transitions of the same kind differing only

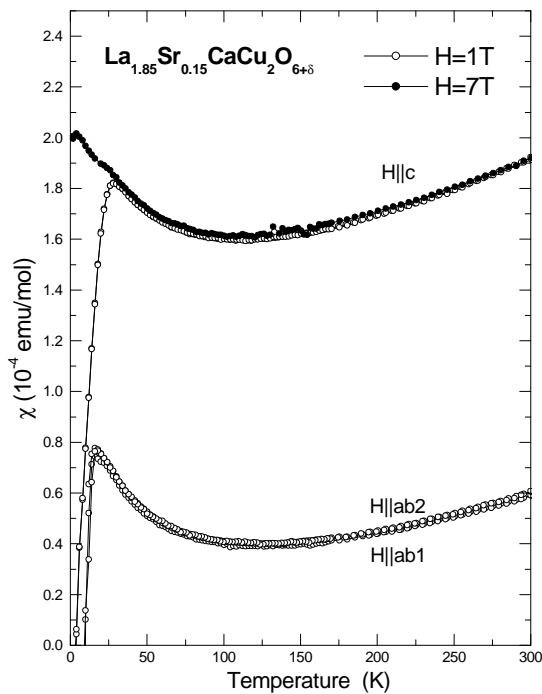


FIG. 12: Static magnetic susceptibility of $\text{La}_{1.85}\text{Sr}_{0.15}\text{CaCu}_2\text{O}_{6+\delta}$ as a function of temperature and different directions of the applied field.

in their critical temperatures, since at ~ 160 K χ first decreases and then again increases at ~ 115 K. Further experiments are needed to clarify the origin of this intriguing sequence of transitions.

Now let us turn to $\chi(T)$ of $\text{La}_{1.85}\text{Sr}_{0.15}\text{CaCu}_2\text{O}_{6+\delta}$, which is shown in Fig. 12. In a field of $H = 1$ T the onset of superconductivity is observed at ~ 25 K for $H \parallel c$ and at ~ 15 K for $H \parallel ab$. At a field of 7 T applied $\parallel c$ superconductivity is suppressed completely. Above T_c the data look similar to that of $\text{La}_{1.9}\text{Ca}_{1.1}\text{Cu}_2\text{O}_{6+\delta}$ in Fig. 10. However, no anomaly is observed at the transition to short-range antiferromagnetic order at ~ 125 K. Interestingly, the increase of χ at high temperatures is steeper than for the Ca-doped sample. This is a clear indication for a shift of the high temperature maximum of the Heisenberg spin susceptibility $\chi_{2D\text{HAF}}$ to lower temperatures, which is consistent with the fact that the hole content in $\text{La}_{1.85}\text{Sr}_{0.15}\text{CaCu}_2\text{O}_{6+\delta}$ is larger and therefore the spin stiffness is smaller than in $\text{La}_{1.9}\text{Ca}_{1.1}\text{Cu}_2\text{O}_{6+\delta}$.⁴¹

D. Discussion

The two major results in this study are (i) the similarity between the thermal evolution of the orthorhombic distortion and antiferromagnetic order for short as well as long-range ordered samples, and (ii) the fact that the antiferromagnetic correlations are commensurate. For a proper interpretation one has to consider the hole concentration, which is known to strongly change the electronic

ground state of high-temperature superconductors.⁷ As mentioned in the introduction, we have estimated the degree of hole doping in our crystals from their optical conductivity in Ref. 27. Both crystals show considerable optical weight at low wave numbers, indicating a significant concentration of holes. In fact, when compared to optical data on $\text{La}_{2-x}\text{Sr}_x\text{CuO}_4$, the hole content appears to be close to the nominal value $p = x/2$, which suggests that the oxygen content δ in our crystals is close to zero.⁵³ Good agreement is also found with optical data in Ref. 54. In particular, the room temperature optical data of our $\text{La}_{1.9}\text{Ca}_{1.1}\text{Cu}_2\text{O}_{6+\delta}$ crystal grown at 1 atm O_2 are nearly identical to that of a grown-in-air $\text{La}_{1.89}\text{Ca}_{1.11}\text{Cu}_2\text{O}_{6+\delta}$ crystal.^{27,54} Corresponding data for our $\text{La}_{1.85}\text{Sr}_{0.15}\text{CaCu}_2\text{O}_{6+\delta}$ crystal grown at 11 atm indicate a higher hole concentration, comparable to $\text{La}_{1.89}\text{Ca}_{1.11}\text{Cu}_2\text{O}_{6+\delta}$ annealed at 20-100 atm.⁵⁴ According to Ref. 54, $\text{La}_{1.89}\text{Ca}_{1.11}\text{Cu}_2\text{O}_{6+\delta}$ is not superconducting when grown in air nor after annealing at 20 atm O_2 , while annealing at 100 atm results in a T_c of 13 K in the resistivity. The presence of weak superconductivity in our Sr-doped crystal and its absence in the Ca-doped one is compatible with this, and shows that the Sr-doped crystal is just on the borderline to the superconducting phase.

If we assume that the hole contents in the crystals are close to the nominal values, then the relatively high Néel temperature in $\text{La}_{1.9}\text{Ca}_{1.1}\text{Cu}_2\text{O}_{6+\delta}$ and onset temperature for short-range order in $\text{La}_{1.85}\text{Sr}_{0.15}\text{CaCu}_2\text{O}_{6+\delta}$ are surprising, when compared to $\text{La}_{2-x}\text{Sr}_x\text{CuO}_4$. However, in the bilayer system $\text{Y}_{1-x}\text{Ca}_x\text{Ba}_2\text{Cu}_3\text{O}_6$ long-range order is suppressed at a higher hole content and spin-glass transition temperatures are higher than in $\text{La}_{2-x}\text{Sr}_x\text{CuO}_4$, as well.⁵⁵ This indicates that in bilayer systems antiferromagnetic order in general is more stable, which is due to the relatively strong coupling between the CuO_2 planes of a bilayer.³⁴ In the case of $\text{La}_{2-x}(\text{Ca},\text{Sr})_x\text{CaCu}_2\text{O}_{6+\delta}$ it seems, however, that additional degrees of freedom may play a vital role, as will be discussed in the next paragraphs.

The intriguing similarity between the temperature dependence of the magnetic Bragg peak and the orthorhombic superlattice peak fuels the idea of a significant magneto-elastic coupling. In particular, we expect that the magnetic inter-bilayer coupling depends on the orthorhombic strain. In the tetragonal high-temperature phase the magnetic inter-bilayer coupling is strongly frustrated, because of the centro symmetric arrangement of spins in adjacent bilayers (cf. Fig. 1). The orthorhombic distortion at low temperature lifts the frustration, thereby triggering 3D antiferromagnetic order. A similar situation exists in the single layer compounds La_2CuO_4 and $\text{Sr}_2\text{CuO}_2\text{Cl}_2$. While La_2CuO_4 becomes orthorhombic below 525 K and orders antiferromagnetically at $T_N = 325$ K, $\text{Sr}_2\text{CuO}_2\text{Cl}_2$ with $T_N = 250$ K stays tetragonal.^{30,41,52,56} It is believed that the orthorhombic strain in La_2CuO_4 is one reason for the higher Néel temperature, since it lifts the frustration of the interlayer cou-

pling.^{52,56,57,58} We mention that early μ SR results on $\text{La}_2\text{CaCu}_2\text{O}_{6+\delta}$ and $\text{La}_2\text{SrCu}_2\text{O}_{6+\delta}$ indicate Néel temperatures higher than 250 K for the undoped system.⁵⁹ On the other hand, in Ref. 18 the structural transition temperature in a $\text{La}_2\text{CaCu}_2\text{O}_{6+\delta}$ powder sample was determined to be ~ 175 K. This means that 3D magnetic order can exist in the tetragonal high temperature phase.⁶⁰ However, in our hole doped $\text{La}_{1.9}\text{Ca}_{1.1}\text{Cu}_2\text{O}_{6+\delta}$ crystal, where T_N is considerably reduced from its maximum value, the structural transition seems to be essential for the stabilization of 3D antiferromagnetic order.

In the case of the $\text{La}_{1.85}\text{Sr}_{0.15}\text{CaCu}_2\text{O}_{6+\delta}$ crystal the magneto-elastic coupling seems to still be active. This conclusion is based on a similar temperature dependence for the peak intensity and correlation length of the structural distortion and antiferromagnetic correlations (cf. Fig. 4). Since in Ref. 18 nearly identical results were found for a $\text{La}_{1.80}\text{Sr}_{0.20}\text{CaCu}_2\text{O}_{6+\delta}$ crystal, we assume that this behavior is intrinsic for samples grown at low oxygen pressure, which are relatively close to the superconducting phase, but not yet good superconductors. However, one has to mention that while neutron diffraction experiments on $\text{La}_{1.80}\text{Sr}_{0.20}\text{CaCu}_2\text{O}_{6+\delta}$ indicate short-range magnetic order below ~ 100 K, muon spin rotation measurements find static order only below 10 K.¹⁸ This shows that for $10 \text{ K} < T < 100 \text{ K}$ the magnetic correlations are not yet truly static. In this respect both $\text{La}_{2-x}\text{Sr}_x\text{CaCu}_2\text{O}_{6+\delta}$ crystals (this work and Ref. 18) qualitatively show a similar behavior as $\text{La}_{2-x}\text{Sr}_x\text{CuO}_4$ in the spin-glass phase.^{61,62,63} However, there are major differences which we believe signal a significant magneto-elastic coupling. First, the “elastic” magnetic intensities we observe in $\text{La}_{1.85}\text{Sr}_{0.15}\text{CaCu}_2\text{O}_{6+\delta}$ below the structural transition at ~ 125 K are much larger than in $\text{La}_{2-x}\text{Sr}_x\text{CuO}_4$ at a comparable hole doping close to the metal insulator transition.⁶³ The onset temperature is much higher and seems to correlate with the structural transition. Moreover, in $\text{La}_{1.85}\text{Sr}_{0.15}\text{CaCu}_2\text{O}_{6+\delta}$ magnetic correlations are commensurate, while they are incommensurate in $\text{La}_{2-x}\text{Sr}_x\text{CuO}_4$.^{18,19,38,63}

Since in $\text{La}_{1.9}\text{Ca}_{1.1}\text{Cu}_2\text{O}_{6+\delta}$ the inter-bilayer exchange seems to couple very clearly to the orthorhombic lattice distortion, it is reasonable to assume that this coupling is at least one reason why in $\text{La}_{1.85}\text{Sr}_{0.15}\text{CaCu}_2\text{O}_{6+\delta}$ the freezing of the short-range magnetic order, as observed by neutron diffraction, reflects the temperature dependence of the structural distortion. In contrast, in $\text{La}_{2-x}\text{Sr}_x\text{CuO}_4$ it is believed that the spin freezing occurs upon the localization of the holes at low temperatures.^{64,65,66} It is very likely that hole localization is relevant in $\text{La}_{1.85}\text{Sr}_{0.15}\text{CaCu}_2\text{O}_{6+\delta}$, also. But whether the structural transition into the orthorhombic phase expedites the hole localization, is unclear. In Ref. 18 it is argued that both structural as well as magnetic disorder

follows from the localization of holes. However, the results on $\text{La}_{1.9}\text{Ca}_{1.1}\text{Cu}_2\text{O}_{6+\delta}$ seem to show quite clearly that it is the orthorhombic structure which stabilizes the antiferromagnetic order. Therefore, we assume that the coupling of the lattice to charge degrees of freedom is not responsible for the structural disorder observed in $\text{La}_{1.85}\text{Sr}_{0.15}\text{CaCu}_2\text{O}_{6+\delta}$. Spin freezing, on the contrary, not only is coupled to charge localization – as is the case in $\text{La}_{2-x}\text{Sr}_x\text{CuO}_4$ – but also to the short-range lattice distortions. The electronic disorder, possibly induced or enhanced by structural disorder, might be responsible for the absence of incommensurate magnetic correlations at low temperatures. As is well known, structural disorder in this bilayer system is caused by the mixed occupation of the metal sites M(1) and M(2), the doping with Sr and Ca as well as by interstitial oxygen O(3) and defects in the oxygen matrix (cf. Fig. 1).^{6,22,67}

IV. CONCLUSION

Structural and magnetic properties of the bilayer cuprates $\text{La}_{1.9}\text{Ca}_{1.1}\text{Cu}_2\text{O}_{6+\delta}$ and $\text{La}_{1.85}\text{Sr}_{0.15}\text{CaCu}_2\text{O}_{6+\delta}$ were studied by means of neutron and X-ray scattering as well as static susceptibility measurements. We observe an intimate connection between antiferromagnetic order and the structural lattice distortion, which we explain in terms of an orthorhombic strain-induced magnetic inter-bilayer coupling. While in the Ca-doped crystal structural distortions and the Cu spins are long-range ordered, the Sr-doped crystal exhibits short-range order as well as weak superconductivity. In both crystals antiferromagnetic correlations are commensurate, i.e., no direct evidence for incommensurate spin stripes is found. However, in $\text{La}_{1.9}\text{Ca}_{1.1}\text{Cu}_2\text{O}_{6+\delta}$ the temperature dependence of the magnetic diffuse scattering as well as the static susceptibility indicate the presence of a spin-glass phase. In $\text{La}_{2-x}\text{Sr}_x\text{CuO}_4$ this type of phase was shown to exhibit a short-range spin stripe order.^{33,38,68} The reasons for the absence of incommensurate spin correlations in particular in $\text{La}_{1.85}\text{Sr}_{0.15}\text{CaCu}_2\text{O}_{6+\delta}$ are not understood, but might result from an inhomogeneity of the charge and spin density, possibly induced by the short-range ordered structural distortions in the orthorhombic phase.

Acknowledgments

We acknowledge support by the Office of Science, US Department of Energy under Contract No. DE-AC02-98CH10886.

¹ R. J. Cava, Science **247**, 656 (1990).

² R. J. Cava, B. Batlogg, R. B. van Dover, J. J. Krajewski,

- J. V. Waszczak, R. M. Fleming, W. F. P. Jr., L. W. R. Jr., P. Marsh, A. C. W. P. James, et al., *Nature* **345**, 602 (1990).
- ³ K. Kinoshita and T. Yamada, *Phys. Rev. B* **46**, 9116 (1992).
 - ⁴ P. W. Klamut, B. Dabrowski, R. Dybziński, and Z. Bukowski, *J. Appl. Phys.* **87**, 5558 (2000).
 - ⁵ E. Pavarini, I. Dasgupta, T. Saha-Dasgupta, O. Jepsen, and O. K. Andersen, *Phys. Rev. Lett.* **87**, 047003 (2001).
 - ⁶ H. Shaked, J. D. Jorgensen, B. A. Hunter, R. L. Hitterman, K. Kinoshita, F. Izumi, and T. Kamiyama, *Phys. Rev. B* **48**, 12941 (1993).
 - ⁷ J. Orenstein and A. J. Millis, *Science* **288**, 468 (2000).
 - ⁸ S.-W. Cheong, G. Aeppli, T. E. Mason, H. Mook, S. M. Hayden, P. C. Canfield, Z. Fisk, K. N. Clausen, and J. L. Martinez, *Phys. Rev. Lett.* **67**, 1791 (1991).
 - ⁹ T. E. Mason, G. Aeppli, and H. A. Mook, *Phys. Rev. Lett.* **68**, 1414 (1992).
 - ¹⁰ S. M. Hayden, G. H. Lander, J. Zarestky, P. J. Brown, C. Stassis, P. Metcalf, and J. M. Honig, *Phys. Rev. Lett.* **68**, 1061 (1992).
 - ¹¹ J. M. Tranquada, B. J. Sternlieb, J. D. Axe, Y. Nakamura, and S. Uchida, *Nature* **375**, 561 (1995).
 - ¹² H. A. Mook, P. Dai, and F. Doğan, *Phys. Rev. Lett.* **88**, 97004 (2002).
 - ¹³ P. Dai, H. A. Mook, R. D. Hunt, and F. Dogan, *Phys. Rev. B* **63**, 54525 (2001).
 - ¹⁴ J. Zaanen, *Nature* **404**, 714 (2000).
 - ¹⁵ S. A. Kivelson, I. P. Bindloss, E. Fradkin, V. Oganessian, J. M. Tranquada, A. Kapitulnik, and C. Howald, *Rev. Mod. Phys.* **75**, 1201 (2003).
 - ¹⁶ J. M. Tranquada, H. Woo, T. G. Perring, H. Goka, G. D. Gu, G. Xu, M. Fujita, and K. Yamada, *Nature* **429**, 534 (2004).
 - ¹⁷ S. M. Hayden, H. A. Mook, P. Dai, T. G. Perring, and F. Doğan, *Nature* **429**, 531 (2004).
 - ¹⁸ C. Ulrich, S. Kondo, M. Reehuis, H. He, C. Bernhard, C. Niedermayer, F. Bourée, P. Bourges, M. Ohl, H. Rønnow, et al., *Phys. Rev. B* **65**, 220507 (2002).
 - ¹⁹ S. Wakimoto, R. J. Birgeneau, M. A. Kastner, Y. S. L. R. Erwin, P. M. Gehring, S. H. Lee, M. Fujita, K. Yamada, Y. Endoh, K. Hirota, et al., *Phys. Rev. B* **61**, 3699 (2000).
 - ²⁰ K. Yamada, C. H. Lee, K. Kurahashi, J. Wada, S. Wakimoto, S. Ueki, H. Kimura, Y. Endoh, S. Hosoya, G. Shirane, et al., *Phys. Rev. B* **57**, 6165 (1998).
 - ²¹ There is evidence that even in the case of $\delta = 0$ some O(3) sites are occupied, which is compensated by a corresponding number of defects on the O(1) or O(2) sites^{3,6,24,25,26}.
 - ²² T. Ohyama, N. Ohashi, O. Fukunaga, H. Ikawa, F. Izumi, and J. Tanaka, *Physica C* **249**, 293 (1995).
 - ²³ H. Deng, C. Dong, H. Chen, F. Wu, S. L. Jia, J. C. Shen, and Z. X. Zhao, *Physica C* **313**, 285 (1999).
 - ²⁴ F. Izumi, E. Takayama-Muromachi, Y. Nakai, and H. Asano, *Physica C* **157**, 89 (1989).
 - ²⁵ J. R. Grasmeder and M. T. Weller, *J. Solid State Chem.* **85**, 88 (1990).
 - ²⁶ P. Lightfoot, S. Pei, J. D. Jorgensen, X.-X. Tang, A. Manthiram, and J. B. Goodenough, *Physica C* **169**, 464 (1990).
 - ²⁷ N. L. Wang, P. Zheng, T. Feng, G. D. Gu, C. C. Homes, J. M. Tranquada, B. D. Gaulin, and T. Timusk, *Phys. Rev. B* **67**, 134526 (2003).
 - ²⁸ T. Freltoft, J. E. Fischer, G. Shirane, D. E. Moncton, S. K. Sinha, D. Vaknin, J. P. Remeika, A. S. Cooper, and D. Harshman, *Phys. Rev. B* **36**, R826 (1987).
 - ²⁹ J. M. Tranquada, D. E. Cox, W. Kunnmann, H. Moudén, G. Shirane, M. Suenaga, P. Zolliker, D. Vaknin, S. K. Sinha, M. S. Alvarez, et al., *Phys. Rev. Lett.* **60**, 156 (1988).
 - ³⁰ P. Böni, J. D. Axe, G. Shirane, R. J. Birgeneau, D. R. Gabbe, H. P. Jenssen, M. A. Kastner, C. J. Peters, P. J. Picone, and T. R. Thurston, *Phys. Rev. B* **38**, 185 (1988).
 - ³¹ P. G. Radaelli, D. G. Hinks, A. W. Mitchell, B. A. Hunter, J. L. Wagner, B. Dabrowski, K. G. Vandervoort, H. K. Viswanathan, and J. D. Jorgensen, *Phys. Rev. B* **49**, 4163 (1994).
 - ³² Correlation lengths were calculated from the peak width using $\xi_a = (\text{HWHM} \times a^*)^{-1}$ and $\xi_c = (\text{HWHM} \times c^*)^{-1}$ where HWHM is the half width at half maximum in reciprocal lattice units of $a^* = 1.64 \text{ \AA}^{-1}$ and $c^* = 0.323 \text{ \AA}^{-1}$, respectively.
 - ³³ M. Matsuda, M. Fujita, K. Yamada, R. J. Birgeneau, Y. Endoh, and G. Shirane, *Phys. Rev. B* **65**, 134515 (2002).
 - ³⁴ J. M. Tranquada, G. Shirane, B. Keimer, S. Shamoto, and M. Sato, *Phys. Rev. B* **40**, 4503 (1989).
 - ³⁵ S. Shamoto, M. Sato, J. M. Tranquada, B. J. Sternlieb, and G. Shirane, *Phys. Rev. B* **48**, 13817 (1993).
 - ³⁶ G. Shirane, S. M. Shapiro, and J. M. Tranquada, *Neutron Scattering with a Triple-Axis Spectrometer* (Cambridge University Press, 2002).
 - ³⁷ In the case that the spins are lying in the CuO_2 planes, for $\mathbf{Q} \parallel \mathbf{c}$ all spins are perpendicular to \mathbf{Q} , while for $\mathbf{Q} \perp \mathbf{c}$ this is generally not the case, depending on the in-plane spin direction and the arrangement of the magnetic domains relative to \mathbf{Q} . As only the spin component perpendicular to \mathbf{Q} contributes to the scattering amplitude, intensity usually increases with increasing l .
 - ³⁸ M. Fujita, K. Yamada, H. Hiraka, P. M. Gehring, S. H. Lee, S. Wakimoto, and G. Shirane, *Phys. Rev. B* **65**, 64505 (2002).
 - ³⁹ Similar scans through the 2D scattering rod at $\mathbf{Q} = (\frac{1}{2}, \frac{3}{2}, \frac{5}{2})$ [with the crystal mounted in the $(h, 3k, 5k)$ zone] are contaminated by Al-powder peaks.
 - ⁴⁰ Y. Okabe and M. Kikuchi, *J. Phys. Soc. Japan* **57**, 4351 (1988).
 - ⁴¹ D. C. Johnston, *Phys. Rev. Lett.* **62**, 957 (1989).
 - ⁴² C. Allgeier and J. S. Schilling, *Phys. Rev. B* **48**, 9747 (1993).
 - ⁴³ I. Terasaki, M. Hase, A. Maeda, K. Uchinokura, T. Kimura, K. Kishio, I. Tanaka, and H. Kojima, *Physica C* **193**, 365 (1992).
 - ⁴⁴ A. N. Lavrov, Y. Ando, S. Komiya, and I. Tsukada, *Phys. Rev. Lett.* **87**, 017007 (2001).
 - ⁴⁵ F. C. Chou, N. R. Belk, M. A. Kastner, R. J. Birgeneau, and A. Aharony, *Phys. Rev. Lett.* **75**, 2204 (1995).
 - ⁴⁶ S. Wakimoto, S. Ueki, and Y. Endoh, *Phys. Rev. B* **62**, 3547 (2000).
 - ⁴⁷ T. Thio, T. R. Thurston, N. W. Preyer, P. J. Picone, M. A. Kastner, H. P. Jenssen, D. R. Gabbe, C. Y. Chen, R. J. Birgeneau, and A. Aharony, *Phys. Rev. B* **38**, 905 (1988).
 - ⁴⁸ M. Hückler, H.-H. Klauss, and B. Büchner, *cond-mat* **0210357** (2002).
 - ⁴⁹ B. Keimer, R. J. Birgeneau, A. Cassanho, Y. Endoh, M. Greven, M. A. Kastner, and G. Shirane, *Z. Phys. B* **91**, 373 (1993).
 - ⁵⁰ T. Thio and A. Aharony, *Phys. Rev. Lett.* **73**, 894 (1994).
 - ⁵¹ T. Thio, C. Y. Chen, B. S. Freer, D. R. Gabbe, H. P. Jenssen, M. A. Kastner, P. J. Picone, N. W. Preyer, and

- R. J. Birgeneau, Phys. Rev. B **41**, 231 (1990).
- ⁵² D. Vaknin, S. K. Sinha, C. Stassis, L. L. Miller, and D. C. Johnston, Phys. Rev. B **41**, 1926 (1990).
- ⁵³ S. Uchida, T. Ido, H. Takagi, T. Arima, Y. Tokura, and S. Tajima, Phys. Rev. B **43**, 7942 (1991).
- ⁵⁴ H. Shibata, T. Watanabe, K. Kinoshita, A. Matsuda, and T. Yamada, Phys. Rev. B **48**, 14027 (1993).
- ⁵⁵ C. Niedermayer, C. Bernhard, T. Blasius, A. Golnik, A. Moodenbaugh, and J. I. Budnick, Phys. Rev. Lett. **80**, 3843 (1998).
- ⁵⁶ M. Greven, R. J. Birgeneau, Y. Endoh, M. A. Kastner, M. Matsuda, and G. Shirane, Z. Phys. B **96**, 465 (1995).
- ⁵⁷ W. Xue, G. S. Grest, M. H. Cohen, and S. K. Sinha, Phys. Rev. B **38**, 6868 (1988).
- ⁵⁸ B. J. Suh, F. Borsa, L. L. Miller, M. Corti, D. C. Johnston, and D. R. Torgeson, Phys. Rev. Lett. **75**, 2212 (1995).
- ⁵⁹ E. J. Ansaldo, C. Niedermayer, H. Glückler, C. E. Stronach, T. M. Riseman, D. R. Noakes, X. Orbadors, A. Fuertes, J. M. Navarro, P. Gomez, et al., Phys. Rev. B **46**, 3084 (1992).
- ⁶⁰ The Néel temperature of pure $\text{La}_2\text{CaCu}_2\text{O}_{6+\delta}$ with $\delta = 0$ is not known.
- ⁶¹ B. Keimer, N. Belk, R. J. Birgeneau, A. Cassanho, C. Y. Chen, M. Greven, M. A. K. A. Aharony, Y. Endoh, R. W. Erwin, and G. Shirane, Phys. Rev. B **46**, 14034 (1992).
- ⁶² M. Matsuda, Y. S. Lee, M. Greven, M. A. Kastner, R. J. Birgeneau, K. Yamada, Y. Endoh, P. Böni, S.-H. Lee, S. Wakimoto, et al., Phys. Rev. B **61**, 4326 (2000).
- ⁶³ H. Hiraka, Y. Endoh, M. Fujita, Y. S. Lee, J. Kulda, A. Ivanov, and R. J. Birgeneau, J. Phys. Soc. Japan **70**, 853 (2001).
- ⁶⁴ H. Takagi, B. Batlogg, H. L. Kao, J. Kwo, R. J. Cava, J. J. Krajewski, and W. F. Peck Jr., Phys. Rev. Lett. **69**, 2975 (1992).
- ⁶⁵ F. C. Chou, F. Borsa, J. H. Cho, D. C. Johnston, A. Lascialfari, D. R. Torgeson, and J. Ziolo, Phys. Rev. Lett. **71**, 2323 (1993).
- ⁶⁶ E. Lai and R. J. Gooding, Phys. Rev. B **57**, 1498 (1998).
- ⁶⁷ K. Kinoshita, F. Izumi, T. Yamada, and H. Asano, Phys. Rev. B **45**, 5558 (1992).
- ⁶⁸ S. Wakimoto, G. S. Y. Endoh, K. Hirota, S. Ueki, K. Yamada, R. J. Birgeneau, M. A. Kastner, Y. S. Lee, P. M. Gehring, and S. H. Lee, Phys. Rev. B **60**, R769 (1999).